Bulletin of the Mineral Research and Exploration

http://bulletin.mta.gov.tr

The relation of seismic velocity and attenuation pattern in the East Anatolian fault zone with earthquake occurrence: Example of January 24, 2020 Sivrice earthquake

Şakir ŞAHİN[a*] and Erdinç ÖKSÜM[a]

[a]*Süleyman Demirel University, Faculty of Engineering, Department of Geophysical Engineering, Isparta, Turkey*

Research Article

Keywords:
EAFZ, Seismic velocity, Attenuation, Tomography.

ABSTRACT

The East Anatolian Fault Zone (EAFZ) is one the main tectonic elements of Turkey, which borders the Anatolian plate from the east. EAFZ, which is NE-SW direction, consists of many fault segments. In the historical and instrumental period, many damaging earthquakes occurred, the largest being 6.8 (Ms) as the 1971 Bingöl earthquake. The last magnitude 6.6 (Ml) (Mw = 6.8) earthquake occurred on January 24, 2020 in Elazığ - Sivrice Hazar - Sincik segment of EAFZ. However, considering the historical and instrumental activity, it is seen that many fault segments are silent. In this study, the silent and active segments, and their seismic velocity (as % Vp and Vp) and attenuation pattern (as Q^{-1}_p) are determined in order to determine the earthquake behavior of EAFZ in the near future. From the results obtained by using the data of the earthquakes that occurred from 2007 to the end of 2019, it was clearly determined that the velocity and attenuation increased on the Hazar - Sincik segment. It has been determined that Vp is 4.08-8.2 km/sec, Q^{-1}_p is ± 0.005 and the frequency dependency varies between 0 - 1.08 along the zone. The variation of velocity and attenuation on the segments where the earthquake occurred and in the silent section were revealed.

Received Date: 23.05.2020
Accepted Date: 09.11.2020

1. Introduction

The East Anatolian Fault Zone (EAFZ) is the largest tectonic member after the North Anatolian Fault Zone in Turkey (NAFZ). The EAFZ, which forms the southern border of the Anatolian Plate with the Arabian plate, joins with the NAFZ in Bingöl - Karlıova. The region where both these tectonic belts join together is the area where the largest stress occur depending on the plate movements in Turkey. The greatest stress occurs here with the pressure exerted by the Arabian plate from south and the Anatolian plate moves westward along the borders of the NAFZ and EAFZ (Allen et al., 2004). In this respect, the EAFZ forms the other border of the Anatolian plate on the land with the NAFZ. The EAFZ, which has a length of 580 km between Karlıova and Hatay, plays a very active role in the geodynamic evolution of the Anatolian block and in the seismicity of Turkey (Arpat and Şaroğlu, 1972; Mc Kenzie, 1976; Taymaz et al., 1991; Herece and Akay, 1992; Şaroğlu et al., 1992; Nalbant et al., 2002; Aksoy et al., 2007; Bulut et al., 2012; Kartal and Kadiroğlu, 2013; Bulut, 2017; Demirtaş and Erkmen, 2019).

In the instrumental period, 1971 Bingöl and 2020 Sivrice earthquakes occurred along the Karlıova - Bingöl and Hazar - Sincik faults respectively with magnitude of 6.5 (Ms) on the EAFZ, which borders the Anatolian Plate from south and consists of many

Citation Info: Şahin, Ş., Öksüm, E. 2021. The relation of seismic velocity and attenuation pattern in the East Anatolian fault zone with earthquake occurrence: Example of January 24, 2020 Sivrice Earthquake. Bulletin of the Mineral Research and Exploration 165, 141-161.
https://doi.org/10.19111/bulletinofmre.824032

**Corresponding author: Şakir ŞAHİN, sakirsahin@sdu.edu.tr*

segments. It was suggested by Demirtaş and Erkmen (2019) that an earthquake should be expected on the parts of Sivrice that continued in the north - east or south - west of the EAFZ, which consists of six fault segments. The very last seismic gaps were formed between the Hazar - Sincik fault and the Bingöl - Karlıova fault after the Sivrice earthquake. In terms of earthquake safety of the cities and large facilities along the EAFZ, it has become important to determine which segments these seismic gaps cover and what kind of earthquake behavior the zone will exhibit in the near future. The seismic velocity change occurring along the zone will help determine the earthquake behavior (Jordan et al., 2011). Considering the ongoing earthquake activity on the EAFZ and finally the 2010 Kovancılar - Elazığ earthquake (Mw = 6.1), it was suggested by Duman and Emre, (2013) that the Pazarcık and Amanos segments had the potential to produce destructive earthquakes in the near future.

Determining the seismic velocity change and attenuation pattern in regions where the earthquake activities are high such as the EAFZ is very important for seismological studies. Seismic velocity diffusion and attenuation within the crust and the mantle are sensitive to heterogeneity in the environment. The seismic attenuation is the decrease in wave energy over time and distance due to the heterogeneity and/or inelastic effects within the crust (Aki and Chouet, 1975; Sato, 1977; Aki, 1980; Pulli, 1984; Sato and Fehler, 1998; Aydın et al., 2020). The transformation of elastic energy into heat or other forms of energy results from the energy dissipation in a heterogeneous environment (Bianco et al., 2002; Abdel - Fattah et al., 2008; Del Pezzo et al., 2006; Sertçelik, 2012). Attenuation studies in time or frequency environments have been performed by various methods using body or surface waves (Pulli, 1984; Ibanez et al., 1990; Mohanty et al., 2009; Mukhopadhyay and Sharma, 2010; Ford et al., 2010; Sharma et al., 2011). The decrease in wave energy depends on the density of the medium and dissipation. The seismic velocity is low and attenuation is high in altered zones and in areas with high volcanic activity, where the fault zones and discontinuities are high. Many studies have been conducted to determine the velocity change and attenuation pattern in the crust in different regions of Anatolia (Akıncı et al., 1994; Akıncı and Eyidoğan, 1996; Eken et al., 2004; Horasan and Boztepe - Güney, 2004; Salah et al., 2007; Sertçelik, 2012; Çağlar, 2019; Demirsıkan et al., 2019; Salah and Şahin, 2019; Aydın et al., 2020).

In this study, the velocity change (%Vp and Vp) and the P wave attenuation (Q_v^{-1}) pattern with the frequency dependency degree (η) according to the characteristics of the environment during the wave propagation were determined the earthquake behavior on the EAFZ January 24, 2020 Sivrice earthquake. The Poisson tomography method was applied for many regions of the world to determine the velocity change and the Coda normalization method was used to determine the seismic attenuation values (Um and Thurber, 1987; Zhao et al., 1992, 1994; Salah et al., 2007; 2011; De Siena et al., 2009; Salah and Şahin, 2019; Demirsıkan et al., 2019; Toker and Şahin, 2019, Şahin and Öksüm, 2020). The elastic wave propagation and attenuation relationships were used to determine these changes. According to the results obtained using the data collected by the end of 2019, it was observed that the %Vp change (Vp values increased) and the attenuation on the Hazar - Sincik fault, where the Sivrice earthquake had occurred, was low. Based on these results, it has been tried to determine what kind of earthquake behavior the other segments on the EAFZ will exhibit.

2. Tectonics and Seismicity of the East Anatolian Fault Zone (EAFZ)

The EAFZ extending between Karlıova in the northeast and Hatay in the southwest, which is approximately 600 km long, consists of 6 different fault segments varying between 50 km to 145 km (Herece, 2003; Demirtaş, 2003; Demirtaş and Erkmen, 2019). These segments, are respectively Türkoğlu - Antakya, Gölbaşı - Türkoğlu, Çelikhan - Gölbaşı, Hazar - Sincik, Palu - Hazar and Karlıova - Bingöl faults as numbered from 1 to 6 in Figure 1. However, the part shown with number 7 not named and it is the intersection of EAFZ fault as shown on the Active Fault Map of Turkey indicated by MTA (2013). On the other hand, the fault shown as number 8 indicates the part where the 2003 Bingöl earthquake occurred (Demirtaş 2003; Demirtaş and Erkmen, 2019). This part is in the same direction with the Yayla Fault (Figure 1).

Structural and geological studies carried out along the EAFZ show that the fault has actively moved in a left - lateral character for the last 3 - 5 million years, with slips around 9 - 40 km (Arpat and Şaroğlu, 1972;

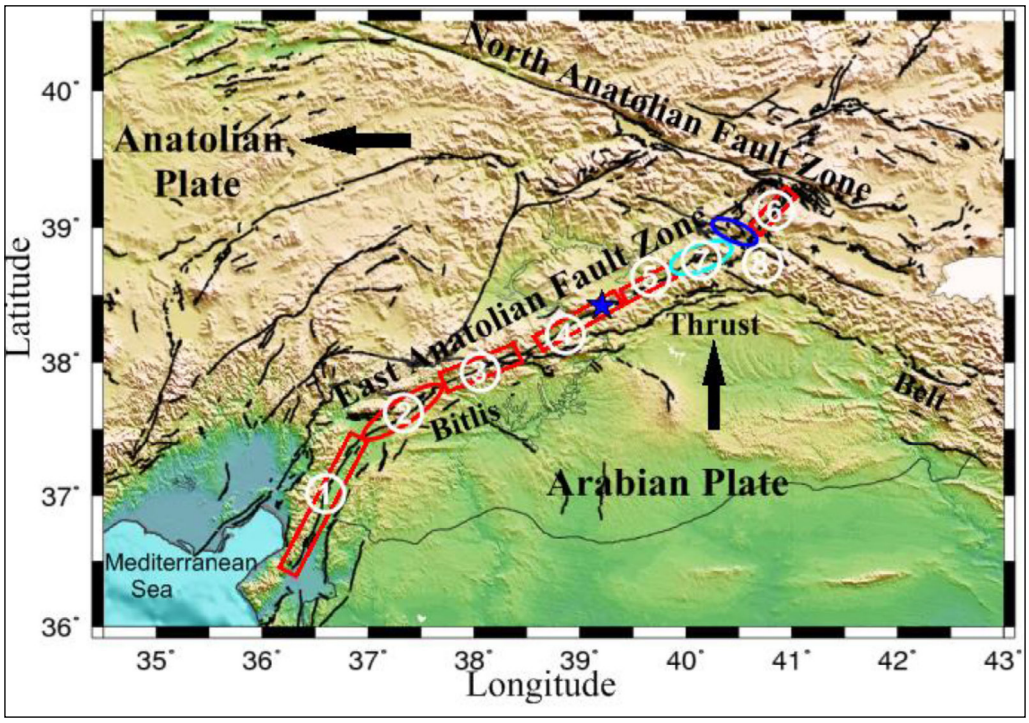

Figure 1- Segments belonging to the Eastern Anatolian Fault Zone (EAFZ) (Demirtaş and Erkmen, 2019) and their tectonic locations. Black arrows show the direction of movement of the plates (Reilinger et al., 2006; Djamour et al., 2011). The segments were shown with red areas, 1. Türkoğlu-Antakya segment, 2. Gölbaşı-Türkoğlu segment, 3. Çelikhan-Gölbaşı segment, 4. Hazar-Sincik segment, 5. Palu-Hazar segment, 6. Karlıova-Bingöl segment. The zone number 7 here is not named, but it is one of the seismic gaps. The number 8 shows the segment where the May 1, 2003 Bingöl earthquake occurred.

Hempton, 1985; Dewey et al., 1986; Allen et al., 2004; Herece and Akay, 1992; Herece, 2003; Aksoy et al., 2007; Demirtaş and Erkmen, 2019). According to the geological data, the age of the EAFZ is expressed as the Upper Pliocene and the average slip rate is 5 - 8 mm/year (Herece, 2003, Demirtaş and Erkmen, 2019). Using the historical earthquake data, it has been determined that there are two seismic gaps between Gölbaşı - Türkoğlu and Palu - Bingöl in EAFZ (Barka and Kadinsky - Cade, 1988; Nalbant et al., 2002; Demirtaş, 2003).

One of the important earthquakes that occurred in the historical period on the segments that form the Eastern Anatolian Fault Zone, numbered as segment 1 above (Figure 1), is the 1822 Antakya Earthquake (Ms = 7.5), which created approximately 200 km of surface rupture (Demirtaş and Erkmen, 2019). The 1866 Karlıova - Bingöl Earthquake (Ms = 7.2), has a surface rupture of approximately 45 km. The May 22, 1971 Bingöl earthquake (Ms = 6.8), took place on the same fault. The historical periods of the earthquakes are respectively; 1872 Amik Lake Earthquake (Ms = 7.2, with approximately 20 km surface rupture) 1874 and 1875 Hazar Lake Earthquakes (Ms = 7.1 and Ms = 6.7 with 45 and 20 km surface ruptures, respectively) and 1893 Malatya Earthquake (Ms = 7.1) (Kartal and Kadiroğlu, 2013; Demirtaş and Erkmen, 2019). The EAFZ, which has a deeper seismogenic zone compared to the NAFZ, produces earthquakes reaching depths of approximately 26 km (Bulut et al., 2012) that started from the NE end of the EAFZ and continued towards SW. The general distribution of historical earthquakes is concentrated in the middle and NE parts of the EAFZ. It is seen that there have not been any devastating earthquakes that formed a surface rupture for the last 500 years on the Gölbaşı - Türkoğlu segment (Figure 1) where the fault folds to the SW.

According to historical records, two damaging earthquakes occurred on the Gölbaşı - Türkoğlu fault in 1114 and 1513 on the EAFZ (segment number 2 in Figure 1). It is stated that after the earthquake that occurred on the segment shown with number 7 in 1789, no significant activity has occurred in this part

(Kartal and Kadiroğlu, 2013; Demirtaş and Erkmen, 2019). After this date, the damaging earthquakes occurred on the Türkoğlu - Antakya fault (segment number 1) in 1822 and 1872, Palu - Hazar (segment number 5) in 1874, Hazar - Sincik in 1875 (segment number 4 where the Sivrice earthquake occurred in 2020), in 1893 and 1905 on the Çelikhan - Gölbaşı segment.

In the instrumental period, damaging earthquakes occurred (Ms = 6.8) on the Karlıova - Bingöl fault (segment number 6) in 1971, in Bingöl (Mw = 6.4) (segment number 8) in 2003 and in Elazığ - Sivrice (Mw = 6.8) on the Hazar - Sincik fault in 2020 (segment number 4) (AFAD, 2020). An earthquake (Mw = 5.2) occurred on the same segment on April 4, 2019. It is observed that earthquakes with Ms = 6.7 and larger occurred along the faults that form the EAFZ in the historical period. The instrumental magnitude of the largest earthquake in the EAFZ in the last century is 6.8 (Ms). If an evaluation is made by considering the mentioned instrumental sizes, it can be said that the middle and NE segment of the EAFZ are more active in the instrumental period. On the other hand, when the historical and instrumental earthquake activities of the EAFZ are assessed together, it is observed that the Gölbaşı - Türkoğlu fault is silent in terms of seismic activity. In addition, the fact that there is no earthquake on segments 2 and 7 (Figure 1) causes that there is a seismically silent phases (Kartal and Kadiroğlu, 2013).

3. Data and Method

In this study, the total of 249,369 P wave arrival time data of 29,687 earthquakes (red circles in Figure 2) was used that had occurred between the latitudes of 35.2 - 41.7 °E and longitudes of 35.9 - 40.1 °N in order to determine the P wave velocity pattern of the Eastern Anatolian Fault Zone. The total of 4,474 digital signals (P phase) of 922 earthquakes (blue circles in Figure 2) was evaluated in order to determine the attenuation pattern that had occurred between the same coordinates. Data were recorded by 40 three - component broadband stations operated by the Kandilli Observatory and Earthquake Research Institute (KOERI) (Figure 3). The location information of stations is given in Table 1. The response function of seismographs in which the earthquakes were recorded is in the range of 0.02 - 100 Hz. The local magnitudes (ML) of the earthquakes used vary between 1 and 6.1 (Figure 2). In determining the attenuation pattern, the signal - to - noise ratio of the earthquake recordings was taken as 1.5 and higher. The beam paths created in determining the beam path distribution velocity values (% Vp and Vp) of the earthquakes used in the study

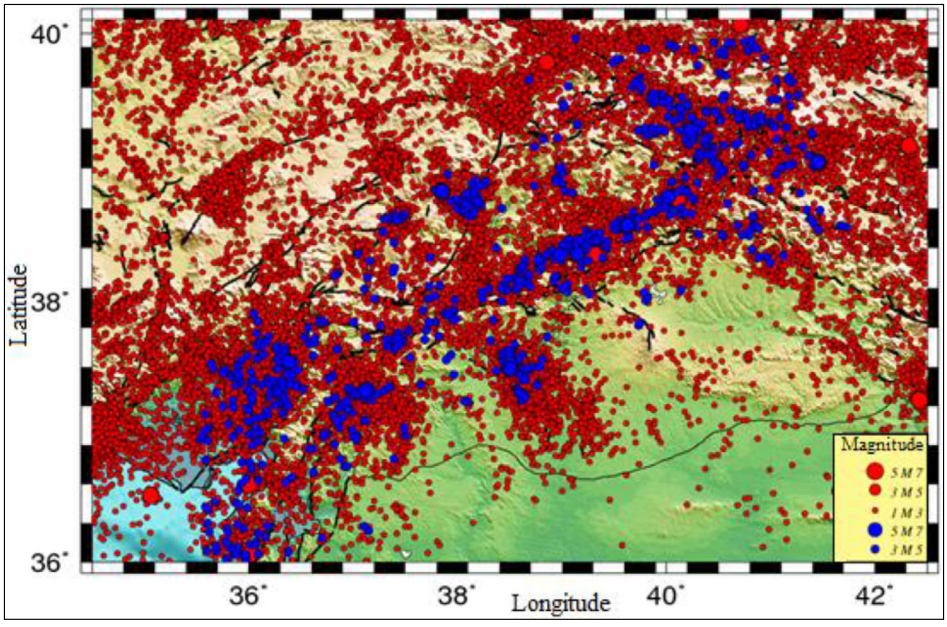

Figure 2- The distribution of earthquakes used in the study. Here, black lines show faults and red circles show the distribution of data used in velocity tomography and blue circles show distribution of earthquakes used in attenuation tomography.

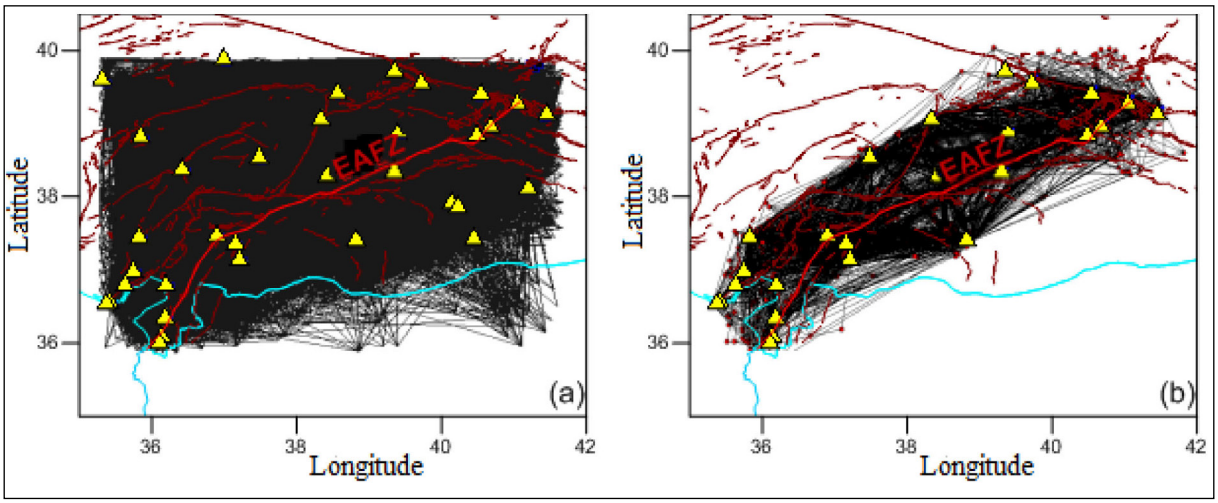

Figure 3- The beam paths created in determining; a) velocity values (% Vp and Vp) and b) attenuation (Q_v^{-1}) values of the earthquakes used in the study. Here, red lines indicate faults (MTA, 2013) and yellow triangles indicate earthquake stations (KOERI, 2020).

Table 1- Location information (KOERI) of the stations where the data used to determine % Vp, Vp and Q_v^{-1} values are recorded.

Station Code	Latitude	Longitude	Height (m)	Station Code	Latitude	Longitude	Height (m)
ARPR*	39.0929	38.3356	1522	BNGB*	38.9913	40.6792	1180
BNN	38.8522	35.8472	1380	CEYT*	37.0107	35.7478	100
DARE*	38.5712	37.4832	1080	DYBB	37.9532	40.1393	657
ERZN*	39.5867	39.7220	1317	GAZ*	37.1722	37.2097	992
ILIC	39.4518	38.5675	1295	KARO*	39.3089	41.0493	1820
KHMN*	37.3916	37.1574	640	KMRS*	37.5053	36.9000	590
KOZT*	37.4805	35.8268	381	KRTD*	36.5934	35.4157	47
KRTS*	36.5730	35.3750	53	MALT*	38.3134	38.4273	1112
MAZI	37.4593	40.4465	1204	PTK*	38.8923	39.3923	1835
SARI	38.4072	36.4182	1673	SVAN	38.1512	41.1985	650
SVRC*	38.3775	39.3060	1680	SVSK	39.9175	36.9925	1630
TAHT*	36.3755	36.1855	278	URFA*	37.4410	38.8213	938
VRTB*	39.1603	41.4558	1498	YEDI*	39.4377	40.5443	1557
YOZ	39.6376	35.3152	1422	BINT*	38.8758	40.4890	1342
BTMT	38.1148	41.2935	854	MYA*	38.3262	38.4253	1050
DIY	37.8958	40.2265	657	EZM	39.9200	41.2800	1870
EZC*	39.7520	39.3535	1500	HTY*	36.1211	36.1378	84
YURE*	36.8258	35.6323	491	DORT*	36.8260	36.1966	27
YAYL*	36.0343	36.1070	1225	ERZM	39.9045	41.3622	23800
ATA5	39.9046	41.2448	18650	EJDE	39.8337	41.3035	29800

*Stations used for attenuation study.

are given in Figure 3a and the beam paths created in determining the attenuation (Q_p^{-1}) values are given in Figure 3b.

The Poisson Tomography method developed by Zhao et al. (1992) was used to determine the seismic velocity pattern of the Eastern Anatolian Fault Zone (EAFZ). In this method, the three - dimensional (3 - D) grid spacing was determined from the inverse solution of the P wave arrival times (Figure 4). The model can be adapted to a general velocity pattern that includes the seismic velocity discontinuities, and 3 - D velocity

changes can be determined throughout the model. The discontinuities represent the known geological boundaries such as Conrad and Moho discontinuities. For this, while defining the initial checkerboard model, the study area was divided into cells (Figure 4), and the velocity distribution in each cell was defined (Figure 5a, b). While the velocity distribution was defined, it was given as the initial velocity model in Table 2 (Kalafat et al., 1987) considering the approximate velocity changes in the study area. Again, Vp / Vs ratio was taken as 1.73 based on in this study. The velocity change at any point in the model is calculated by linear

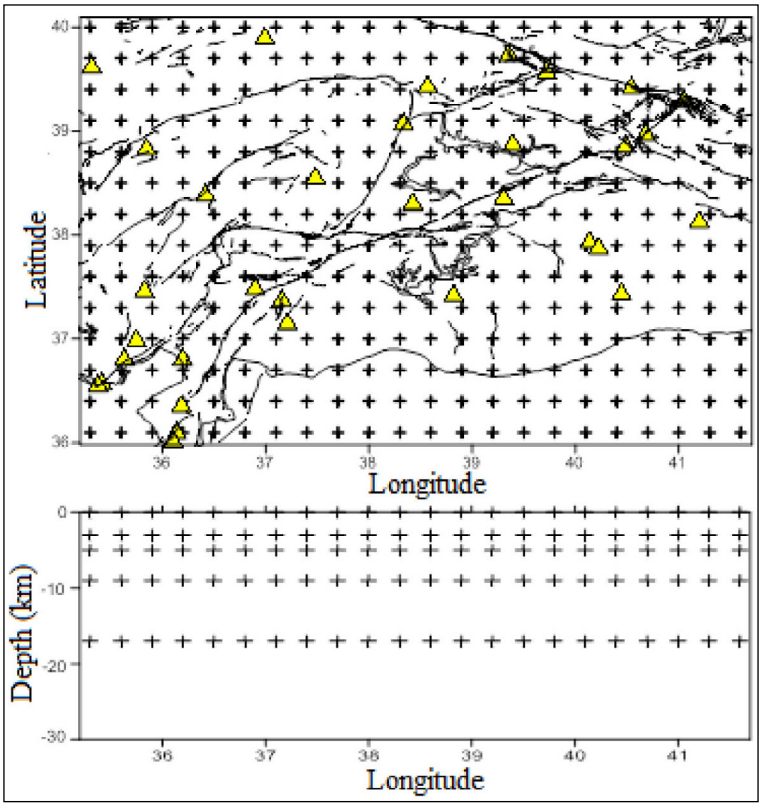

Figure 4- Position of grid spacing in horizontal (top) and vertical (bottom) directions. The grid spacing was taken as 0.3° * 0.3° in the horizontal direction and as -3, -5, -9 and -17 km depths in the vertical direction.

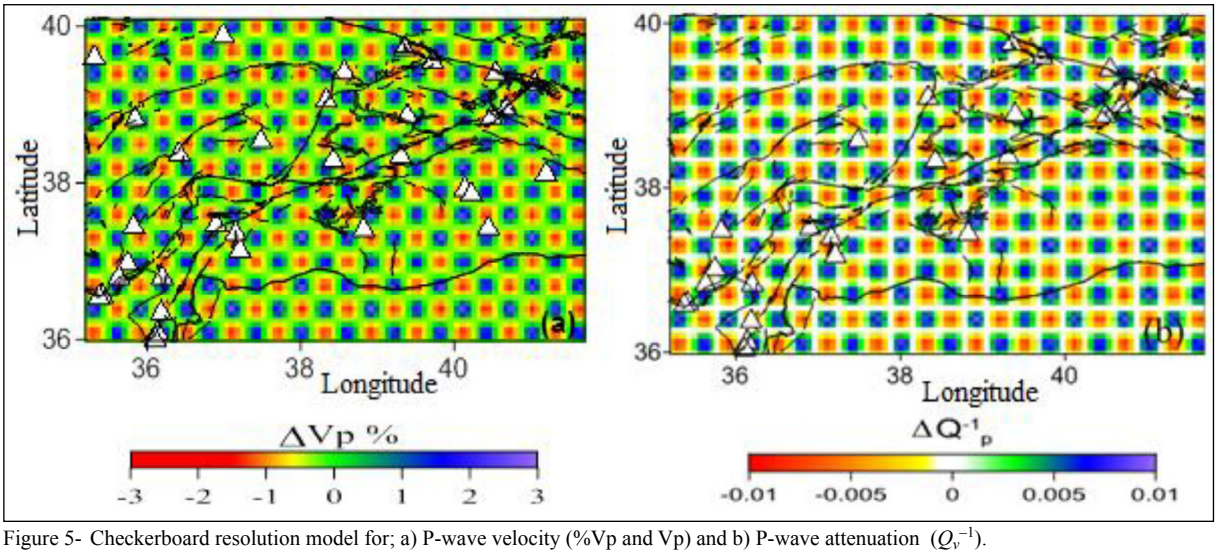

Figure 5- Checkerboard resolution model for; a) P-wave velocity (%Vp and Vp) and b) P-wave attenuation (Q_v^{-1}).

Table 2- Initial velocity model used to determine % Vp, Vp and Q_v^{-1} values (Kalafat et al., 1987).

Depth (km)	Vp (km/sec)	Vs (km/sec)
0	4.50	2.60
5.4	5.91	3.41
31.6	7.80	4.51
89.2	8.30	4.80

interpolation of the velocity changes at eight nodes surrounding that point. The iterative Pseudo Bending technique was used to calculate the arrival times and ray paths, accurately (Um and Thurber, 1987; Zhao et al., 1992). This technique is a three - dimensional ray tracing method. The detection of beam paths is based on Snell's law. In this method, the station heights were also taken into account which is defined as the Poisson tomography.

At the stage of determining the initial model for the checkerboard test (Figure 5a, b), many trials were conducted by changing the horizontal and vertical cell spacing and velocity distributions, considering the width of the study area and the possible velocity changes in the region. As a result of these trials, the study area was gridded at 0.3° * 0.3° in the horizontal direction and as 1 km interval in the vertical direction. The model depth was defined up to 30 km in order to complete the beam paths in the study area. The amplitudes and P wave velocity anomalies for attenuation anomalies were determined as ± 3% and ± 0.01, respectively (Figure 5a, b).

Tomographic methods are based on the inverse analysis of arrival times of seismic waves within the parameters specified above (Zhao et al., 1994). In visualizing the crust and mantle structure, the geometric shape of the structure is taken into account in the model parameterization stage (Thurber, 1987). The TOMOTOOLS (Farouk and Zhao, 2006) software obtained with the interface created for the code of the TOMOG3D (Zhao et al., 1992) software was used to determine the structure of P and S velocities. This software was designed to determine the crust and upper mantle velocity structures from the inverse resolution of arrival times of the recorded local earthquakes. TOMOTOOLS enables the determination of existing complex discontinuities in a realistic model and obtaining 3 - D changes between the velocities.

The vertical component P wave was used to determine the three - dimensional attenuation pattern by tomographic method. For this, the signals that were windowed on the P phase and the noise selected 5 seconds before the 2 second time interval were selected and the spectral amplitudes of the selected signals were determined. The ratio of P wave and noise spectral amplitudes was calculated. The selection of signal and noise is given in Figure 6. The Coda Normalization Method used in the study is based on spectral amplitude ratios. Based on this method, the attenuation patterns were determined with the Matlab - based MuRATv.2 software (De Siena et al., 2016, 2017) developed by De Siena et al. (2009).

This software was developed, which is based on the approach of the coda normalization method model by Del Pezzo et al. (2006), Aki (1980) and Frankel et al. (1990). The method applied is based on the assumption that the average source size and ground amplification calculated from many earthquake data spread in different directions are independent of the source - receiver direction and the average value varies geographically (Aki, 1980). The (Q_p^{-1}) values, which are P wave attenuation parameters, are calculated from the decrease of the P wave amplitude of the crust caused by inelastic conditions at each station (Aki, 1980; Frenkal et al., 1990). For this purpose, 2 - second windows (Δt = 2 seconds) on the P wave and noise were selected and calculated as seen in Figure 6. This process is based on the approach of (Aki, 1980; Frenkal et al., 1990).

$$\langle Ln\{D^{\gamma} * A_P(f)/A_G(f)\}\rangle = a - b * D \quad (1)$$

Here; D is the source - receiver distance, g is the geometric radiation effect, A_p *(f)* is the spectral amplitude of the P wave and A_G*(f)* is the noise spectral amplitude. The coda normalization method is widely used in the calculation of attenuation in the earth crust independent of soil and instrumental transfer function (Aki, 1980; Sato and Fehler, 1998; Şahin and Alptekin, 2003; Aydın et al., 2012).

The P wave attenuation in the EAFZ in Del Pezzo et al., (2006) model was calculated for certain depths along each wave path (Figure 4). The energy reduction relation used for this is given by the formula of;

$$\frac{E_{ij}(f,r)}{E^G(f,t)} r_{ij}^2 = \frac{1}{P(f,t_G)} exp\left[-2\pi f \int \frac{dl}{v(l)Q_P^{ij}(l)}\right] \quad (2)$$

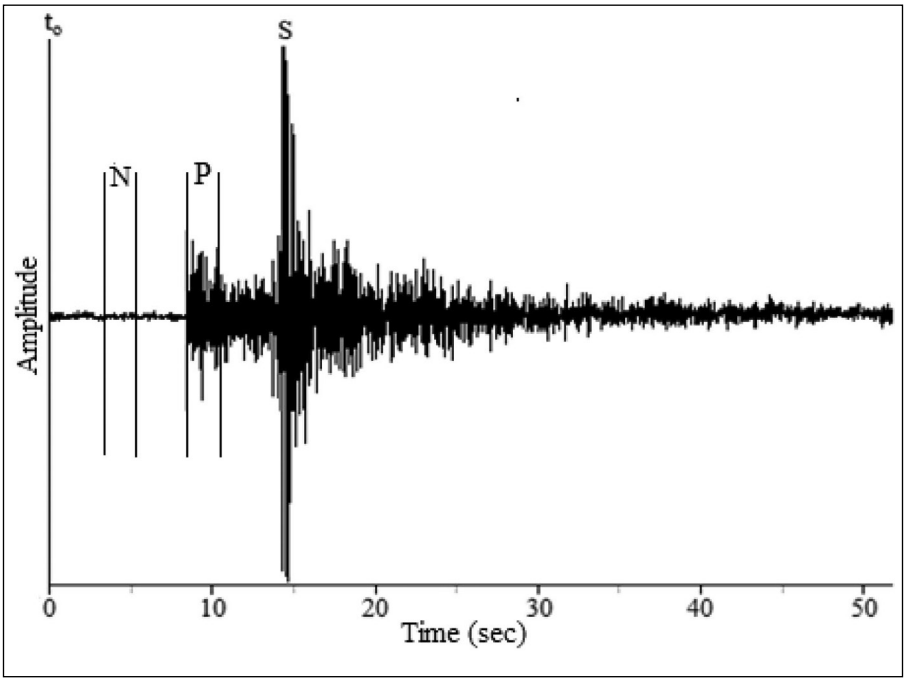

Figure 6- Representation of P and S wave phases on the signal. Here, P and N is the 2-second P wave selected to determine the attenuation parameters, and t_0 indicates the time of occurrence of earthquake.

With the application of linear integral by taking the logarithms of both sides, the following formula is obtained;

$$d_k^G = \frac{1}{2\pi f} \ln\left(\frac{1}{P(f,tc)}\right) - \sum_{b=1}^{N-cell} l_{kb}\, S_b Q_b^{-1} \quad (3)$$

Here the d_K^G value gives the logarithm of the P wave and the noise spectral ratio determined for the beam length and is gridded for the given metric range. The N cells gridded is the total number of blocks traversed by the beam. Here, the S_b attenuation value is the k^{th} beam path length that cuts the block b, which is characterized by the $l_{kb}\,Q$ quality factor, and k is the wave path index between the earthquake focus and the station.

The equation (3) can be rewritten so that the average attenuation value of each b block in the studied area is Q_b^{-1} and increasing dQ_b^{-1}. As a result;

$$\tilde{d}_k^G = \sum_{b=1}^{N-cell} l_{kb}\, S_b \quad Q_b^{-1} \quad (4)$$

From here the following formula is obtained (De Siena et al., 2009).

$$\tilde{d}_k^G = \frac{1}{2\pi f} \ln\left(\frac{1}{P(f,tc)}\right) - \tilde{d}_k^C - Q_P^{-1} \sum_{b=1}^{N-cell} l_{kb}\, S_b \quad (5)$$

From here, Q_p^{-1} values are calculated for a certain frequency value in each cell. In this study, the frequency value was taken as 18 Hz.

With the Coda Normalization Method, the spectral amplitude ratios of the P waves and the noise window are displayed as a function of the distance of earthquakes to the earthquake station, and the attenuation pattern is calculated from the decrease of the amplitude ratio (Aki, 1980; Frenkal et al., 1990). In the last stage, the average Q_v^{-1} wave attenuation parameter for each cell was determined by proportioning the spectral amplitude values of the P wave. In this way, the discontinuities in the crust and the continuity of structures were determined. In the method developed by De Siena et al. (2009) (MuRATv.2), P and S wave attenuation is determined depending on the velocity structure in the environment (De Siena et al., 2016; 2017; Şahin and Öksüm, 2020).

4. Discussion

Checkerboard test was applied to determine the resolution in determining the rate and attenuation pattern on the EAFZ (Figures 7 and 8). Initially, the

checkerboard resolution model was created (Figure 5a, b) and the resolution tests were applied according to the velocity model given in Table 2. The parameters applied for the matrix before the inverse solution are determined according to the station and earthquake distribution, the region examined and the number of rays. For this reason, the special parameterization is made for each study area during the synthetic tests stage and its effects on the results are investigated. The study area in the checkerboard test is divided into square / rectangular prisms of certain sizes (Figure 5a, b). To each of these prisms negative / positive or low / high attenuation values are assigned. Then, the noise is added to the synthetic arrival times considering the phase reading errors and as a result of the inverse solution, it is checked whether these prisms can be synthetically recovered. If the desired resolution is not obtained, then the test is repeated by changing the dimensions of the square / rectangular prism (Özer et al., 2018). In this study, the prism dimensions for the P wave were designed to be 0.3° *0.3°, ± 3% for the DVp% values and ± 0.01 ΔQ_p^{-1} values for the attenuation pattern (Figure 5a, b). It was considered as if the seismic model produced by synthetic arrival times had not been known and the inverse process was performed using a new initial model. In this way, the checkerboard model used in the beginning was tried to be obtained. Checkerboard resolution maps were obtained based on the initial crustal depth and velocity model (Figures 7 and 8). In addition, the resolution sections were taken along the fault zone and perpendicularly (Figures 12, 15 and 18a, d). The resolution level of the designed resolution model at different depths for the P wave velocity and attenuation was examined. According to the results obtained, it was seen that the resolution for the P wave velocity values on the surface could be obtained at 30 km depth, but for P wave attenuation, the resolution could be obtained down to 17 km. In both methods, it was observed that the resolution was low at 2 km depth from the surface, and the resolution increased after 3 km. Based on these results, depth maps were obtained for both methods depending on the resolution at 3, 5, 9 and 17 km. When the map is divided into cells consisting of positive and negative anomalies, it was observed that the results with high resolution were obtained at these

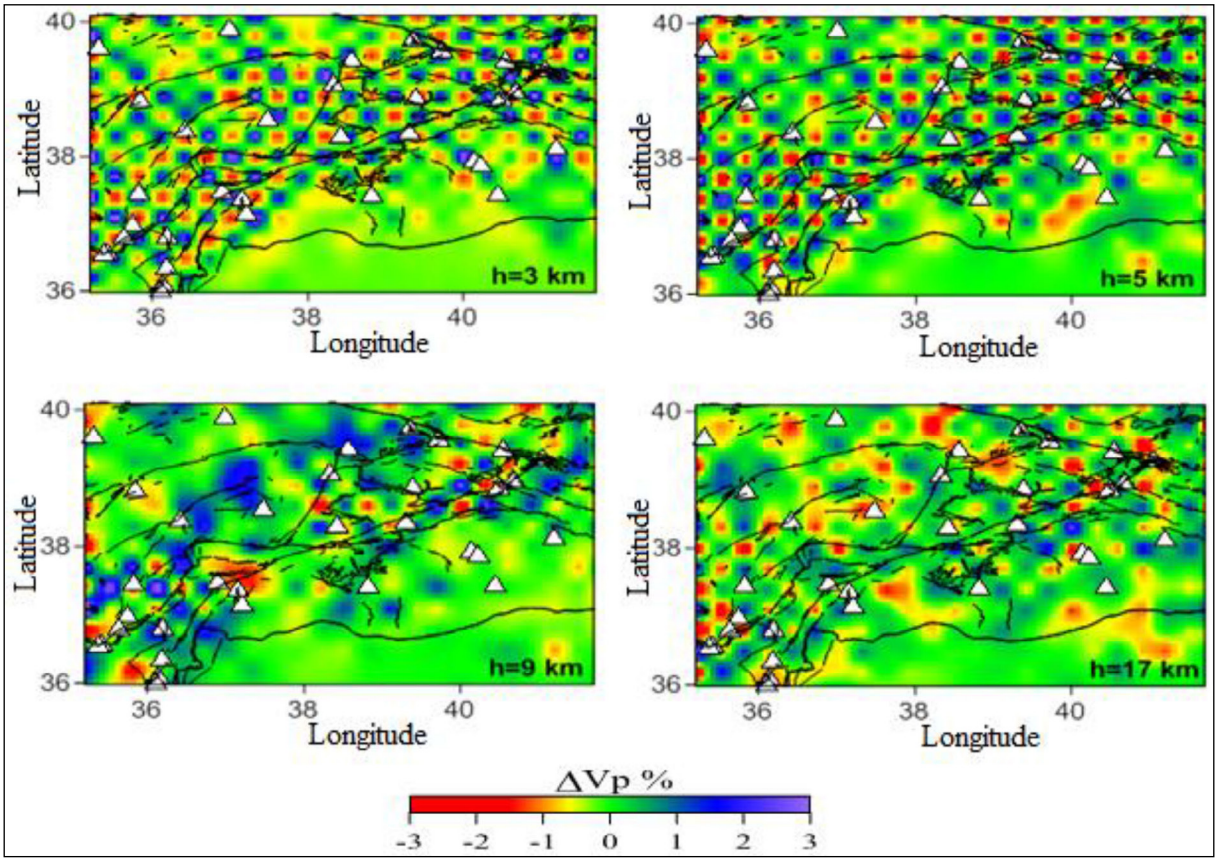

Figure 7- P wave velocity distribution checkerboard test results (% Vp and Vp) at 3km, 5 km, 9 km and 17 km depths.

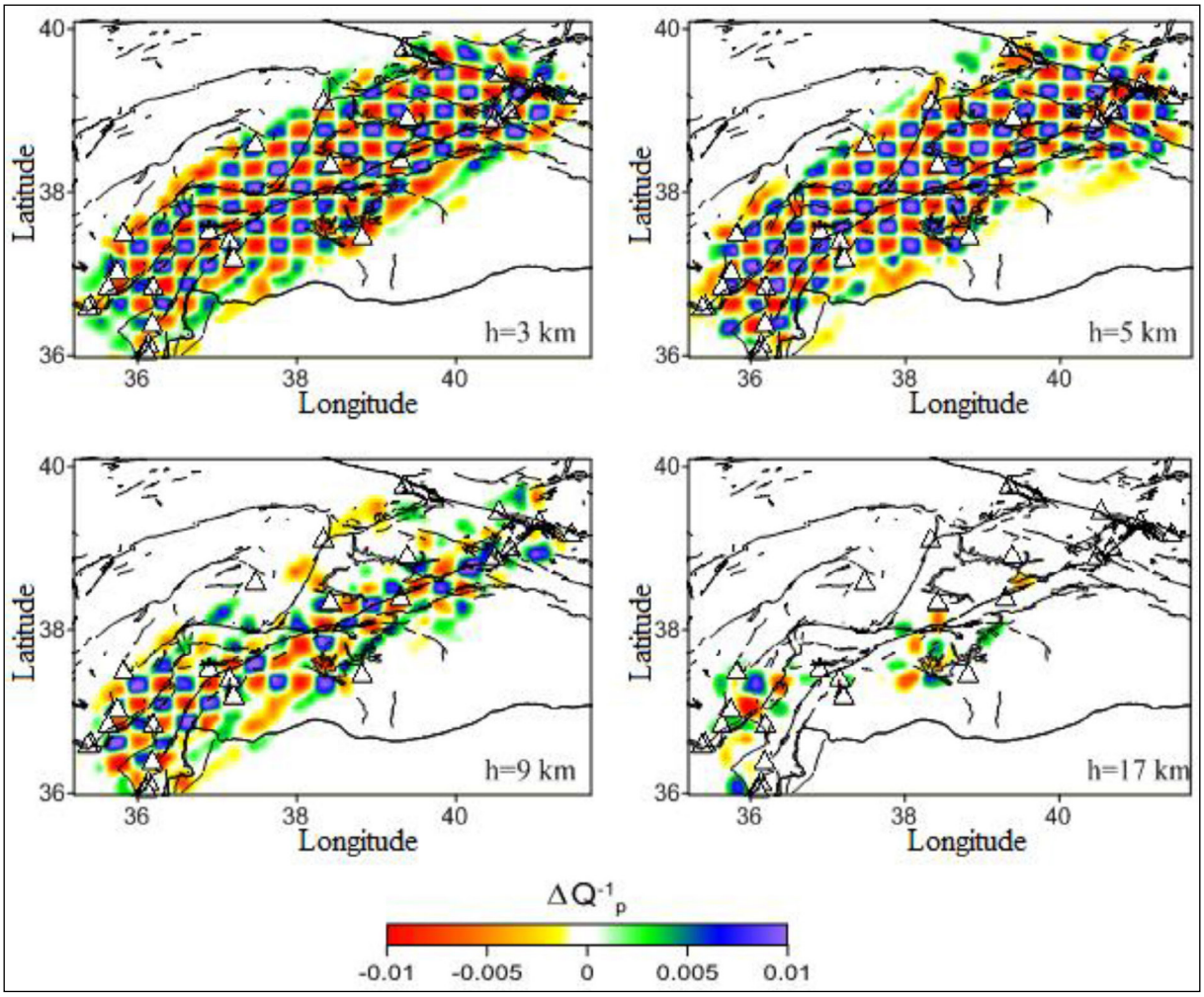

Figure 8- Checkerboard test results for P wave attenuation (ΔQ_v^{-1}) at 3km, 5 km, 9 km and 17 km depths.

depths. According to the checkerboard results, the resolution decreases in the number of rays due to the low number of stations and rare earthquakes, and the low intensity of earthquakes as going towards deeper parts. The resolution changes after 9 km depth for the P wave velocity changes obtained in the checkerboard test results, and after 5 km depth for the attenuation change. The amount of error in depth for determining the change in the P wave velocity is ± 1.24 km and ± 0.9 km for determining the attenuation values. The resolution of the P wave velocity change is higher. Here, the velocity change values were calculated from earthquake data showing both spatial distribution and along the fault, and attenuation values were obtained only from earthquakes occurring along the EAFZ. The deeper adoption of P wave velocity changes in depth sections is due to the long and more beam paths. Therefore, a difference occurs in the deep alignment of the beam path.

By applying the inverse solution to the arrival times of P waves of the earthquakes occurring between longitudes of 35.2° - 41.7° E and latitudes of 35.9° - 40.1° N in the Eastern Anatolian Fault Zone (EAFZ), the three - dimensional velocity changes and the attenuation pattern along the EAFZ were determined (Figures 9-11). The % Vp, Vp and ΔQ_p^{-1} values were correlated with the depth given above and the distribution of earthquakes in the underlying layer (Figures 9-11). According to the results, it was observed that the velocity change and attenuation was low in the Hazar - Sincik segment (segment 4 in Figure 1) where the January 24, 2020 Sivrice earthquake had occurred, and the Vp velocity is the same as the peripheral units down to a depth of 7 - 8 km, but lower in deeper parts with respect to the environment (Figures 9-10).

Although % Vp, Vp and ΔQ_p^{-1} values show regional distribution in parts close to the earth, it is noteworthy

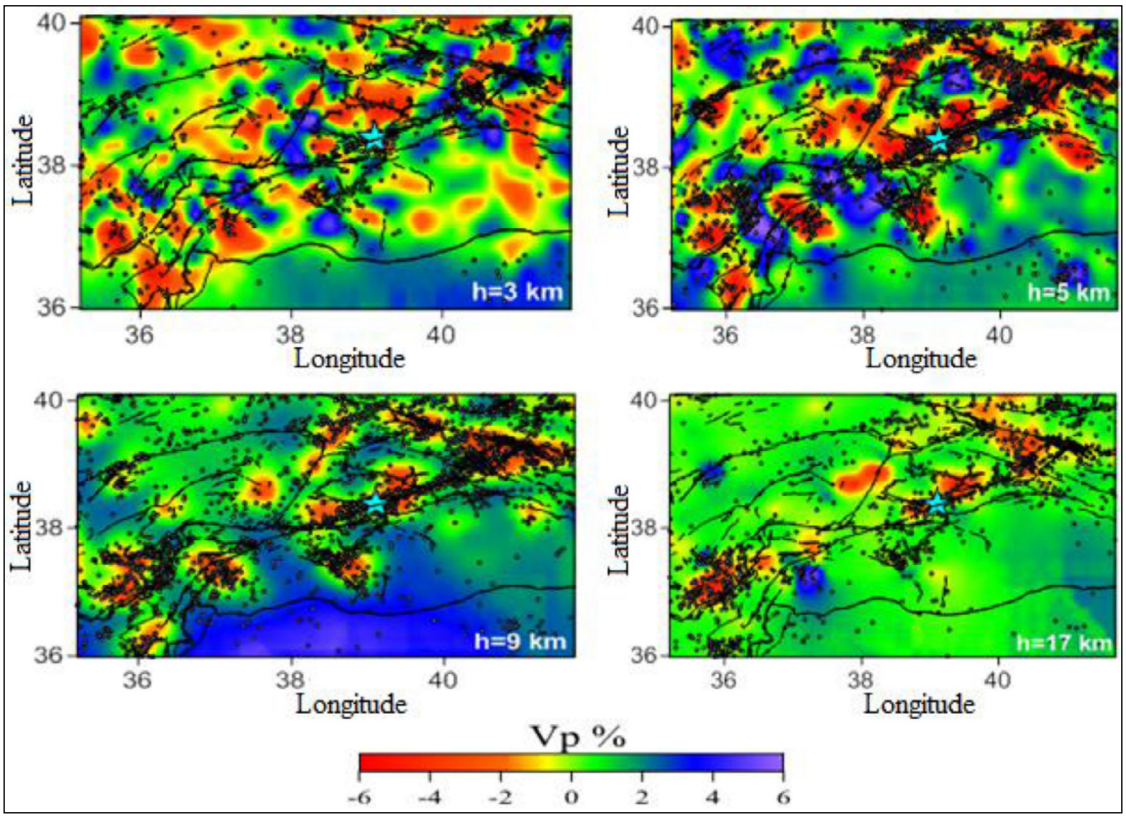

Figure 9- Spatial distribution of P wave velocity change (Vp%) values at 3, 5, 9 and 17 km depths and their relation with the tectonic structure. The points here show the focal distribution of earthquakes at the depths given.

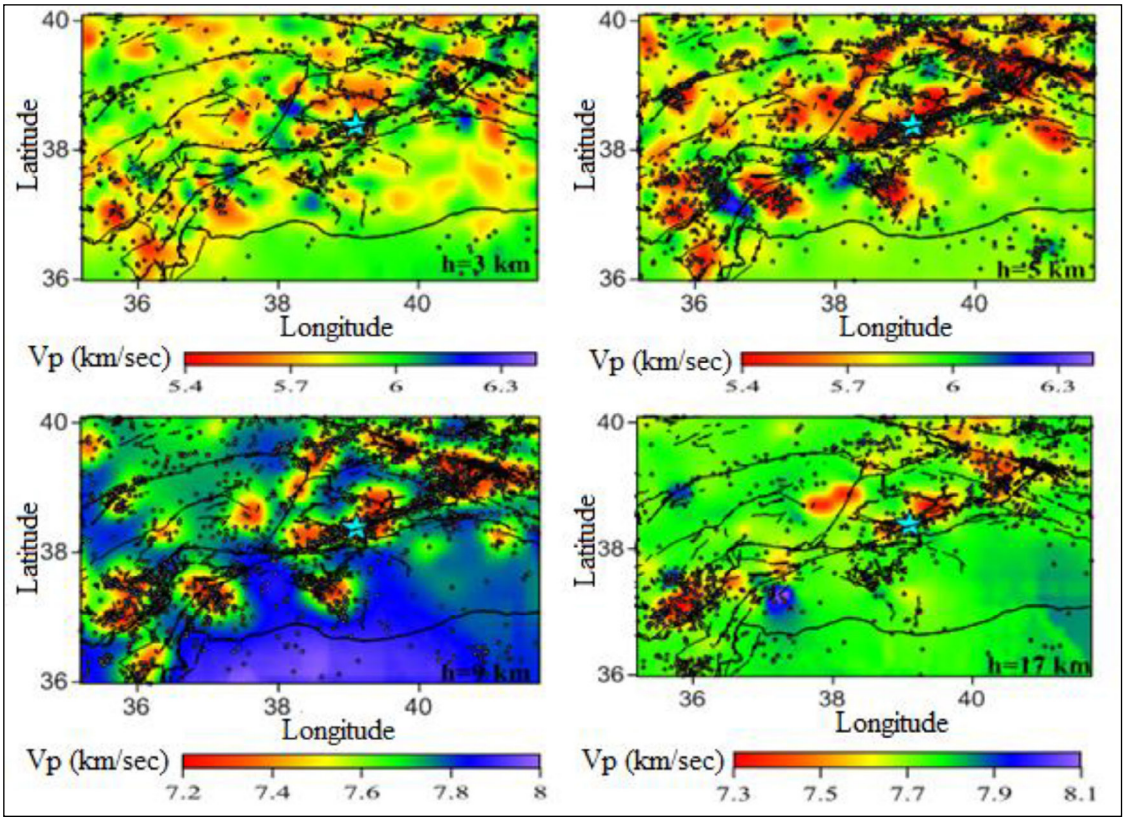

Figure 10- The spatial distribution of P wave velocity (Vp) values at 3, 5, 9 and 17 km depths and their relationship with the tectonic structure. The points here show the focal distribution of earthquakes at the depths given.

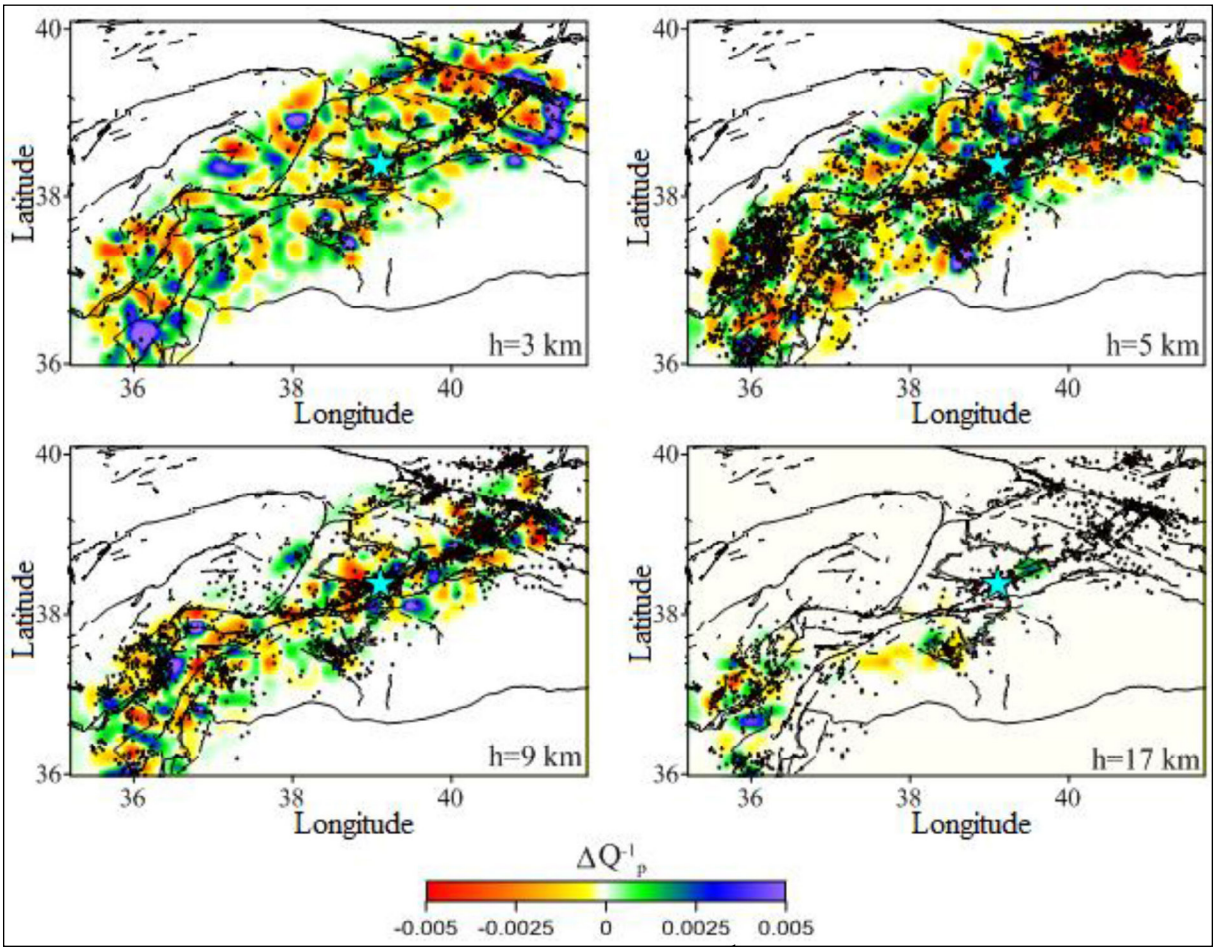

Figure 11- The spatial distribution of P wave attenuation (ΔQ_v^{-1}) values at 3, 5, 9 and 17 km depths and their relationship with the tectonic structure. The points here show the focal distribution of earthquakes at the depths given.

that they show a change due to faults as going deeper. The variation starts from the 5th kilometer depending on the fault planes. At this depth, the decrease in % Vp values (Figure 9) and the increase in Vp values (Figure 10) are particularly concentrated on the Hazar - Sincik fault. This situation continues down to 30 km depth (Figures 9 and 10). In the results obtained by geodetic studies too, it was suggested that the slip had reached a depth of 20 km (Melgar et al., 2020). However, there is observed an increase in % Vp and ΔQ_p^{-1} values in the NAFZ in the Karlıova region. In addition, the existence of similar situation was detected in Hatay, which is on the Türkoğlu - Antakya segment where two important earthquakes had occurred in 1822 and 1872, in the Adana Basin where the 1945 and 1998 earthquakes had occurred, in Gölbaşı - Türkoğlu, where the 1114 and 1513 earthquakes had occurred, and on Karlıova - Bingöl segments where the 1866 and 1971 earthquakes had occurred (İmamoğlu and Çetin, 2007; Yalçın et al., 2012; Demirtaş and Erkmen, 2019; Jamalreyhan et al., 2020). It was observed that the % Vp, Vp and ΔQ_p^{-1} values obtained were compatible with the heat flux values (Çırmık, 2018). It is possible to say that the mantle material approaches the surface in this region. It was determined that the slip velocity on the EAFZ was mostly over the Hazar - Sincik segment and the velocities obtained from the fault surround were concentrated in the Bingöl - Karlıova region (Bulut, 2017).

Two separate sections in two different directions along the EAFZ (Figure 12-17) as being perpendicular to the Hazar - Sincik segment (from the 24 January 2020 Sivrice earthquake epicentre) (Figure 18) were taken and the changes of % Vp, Vp, ΔQ_v^{-1} and frequency dependency degree (h) were determined**.** It was seen that the deep seated earthquakes that occurred along the EAFZ in the instrumental period concentrated on this segment. The increase of h up to 1.08 on this segment indicates that seismotectonic

activity is high here (Figure 16). In sections taken perpendicular to the EAFZ as given in Figure 17, it was observed that the effects of velocity and attenuation were on the Hazar - Sincik segment where the deepest Sivrice earthquake occurred on January 24, 2020. On the other hand, there is an earthquake clustering on Gölbaşı - Türkoğlu (segment number 2), Bingöl - Karlıova (segment number 6) and the unnamed segment number 7 on the EAFZ. However, it is possible to say that the cluster on segment number 7 is the Bingöl earthquake that occurred on May 1, 2003 and its aftershocks.

In addition, a 3 - dimensional cross - section was taken to determine the change of % Vp, (ΔQ_v^{-1}) and η along the EAFZ (Figures 19-21). The compatibility of %Vp with (ΔQ_v^{-1}) values in the horizontal cross - section maps and each other at the intersection points of the lines are noteworthy. Based on the cross - sections and examination of the earthquake focal

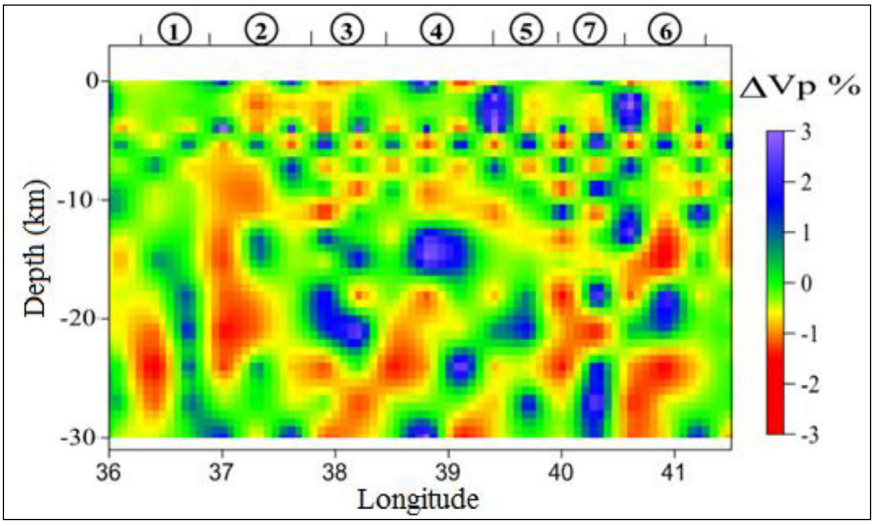

Figure 12- Checkerboard test result for P wave attenuation (ΔQ_v^{-1}) along the EAFZ. Segments on the cross section; 1) Türkoğlu-Antakya segment, 2) Gölbaşı-Türkoğlu segment, 3) Çelikhan-Gölbaşı segment, 4) Hazar-Sincik segment, 5) Palu-Hazar segment and 6) Karlıova-Bingöl segment. The number 7 here is not named, and it is one of the seismic gaps present in the region.

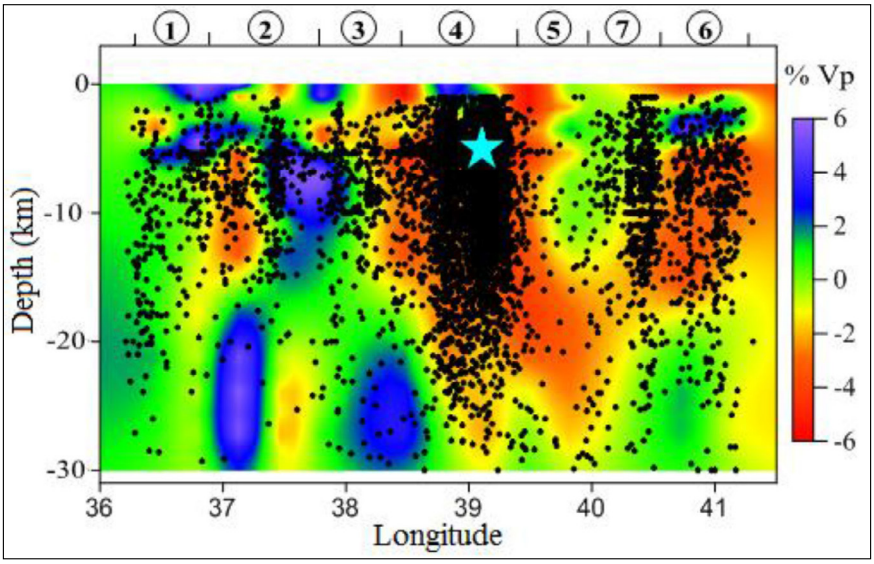

Figure 13- %Vp change along the EAFZ. Here, the black dots indicate the focal distribution of earthquakes along the zone, and the blue star indicates the focal depth of the January 24, 2020 Elazığ-Sivrice earthquake. Numbers on the cross section are the same as in Figure 12.

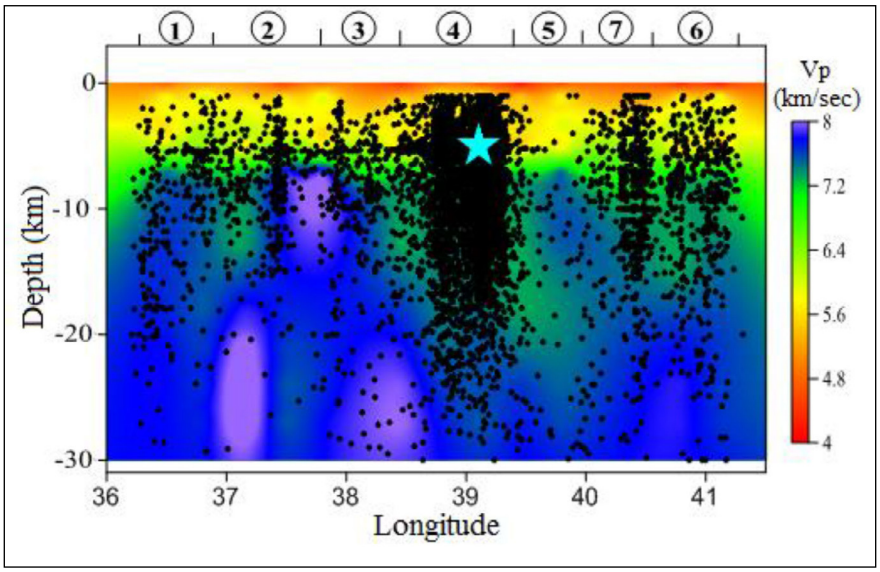

Figure 14- Vp (km/sec) change along the EAFZ. Here, the black dots indicate the focal distribution of the earthquakes occurring along the zone, while the blue star indicates the focal point of the January 24, 2020 Elazığ-Sivrice earthquake. Numbers on the cross section are the same as in Figure 12.

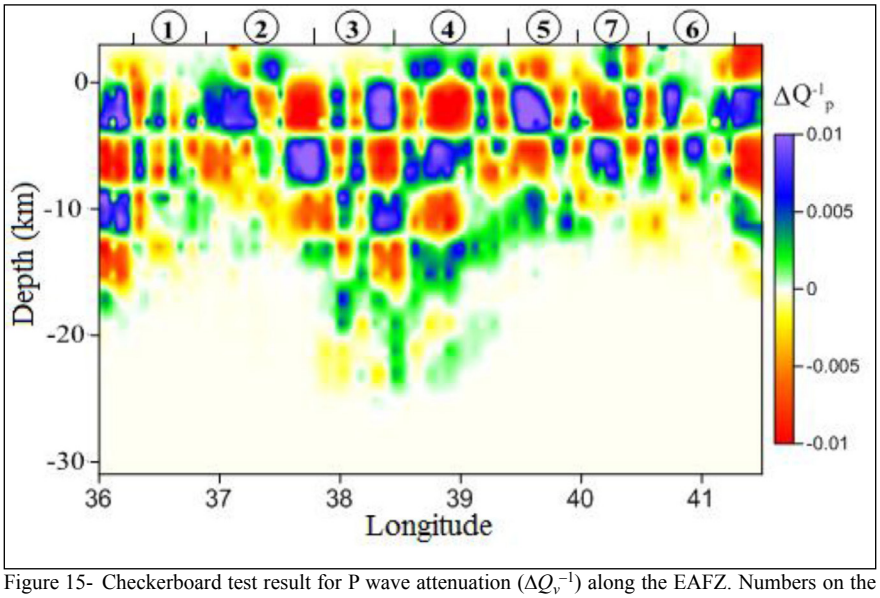

Figure 15- Checkerboard test result for P wave attenuation (ΔQ_v^{-1}) along the EAFZ. Numbers on the cross section are the same as in Figure 12.

depths, the EAFZ depth is estimated to be around 36 km. It was observed that the %Vp, Vp, **(ΔQ_v^{-1})** values obtained were compatible with seismogenic zones and crustal attenuation determined in the region (Turkelli et al., 2003; Zor et al., 2007).

It is observed that the %Vp change decreases to 30 km, ΔQ_v^{-1} value decreases to 17 km and the frequency - dependent change decreases down to 15 km in vertical sections obtained along the EAFZ. It is seen that all three values reach the deepest point in the Hazar - Sincik segment (Figures 12-17). On the other hand, the decrease of the %Vp and the increase of the Vp values were detected in the segment 6 and in the segment 2, close to the boundary of segment 1 (Figures 13 and 14). There was observed a change on the boundary region of the Dead Sea Fault and the EAFZ in ΔQ_v^{-1} values, and it is compatible with the change in velocity (Figure 16). A similar situation is also observed in the values of h (Figure 17). It was

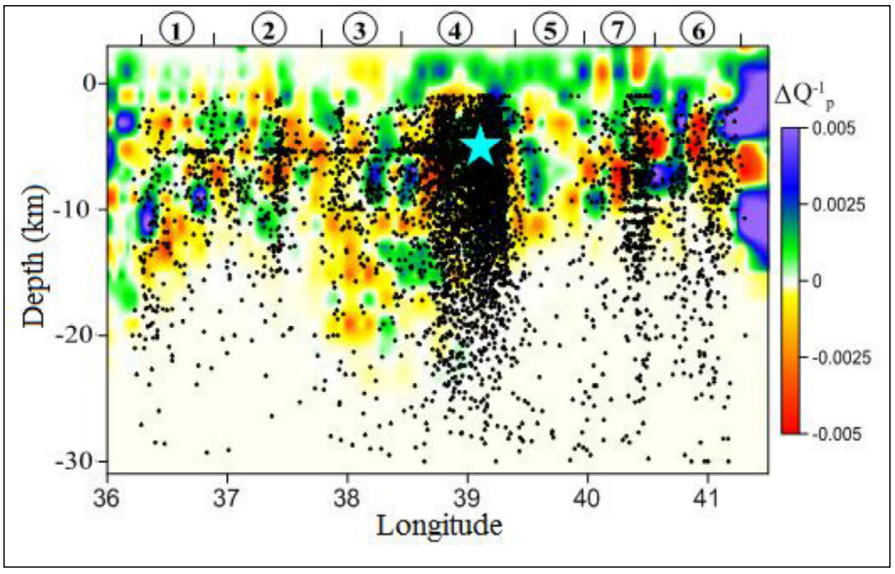

Figure 16- The variation of attenuation (ΔQ_v^{-1}) values along the EAFZ. Here, the black dots indicate the focal distribution of earthquakes along the zone, and the blue star shows the focal depth of the 24 January 2020 Elazığ-Sivrice earthquake. Numbers on the cross section are the same as in Figure 12.

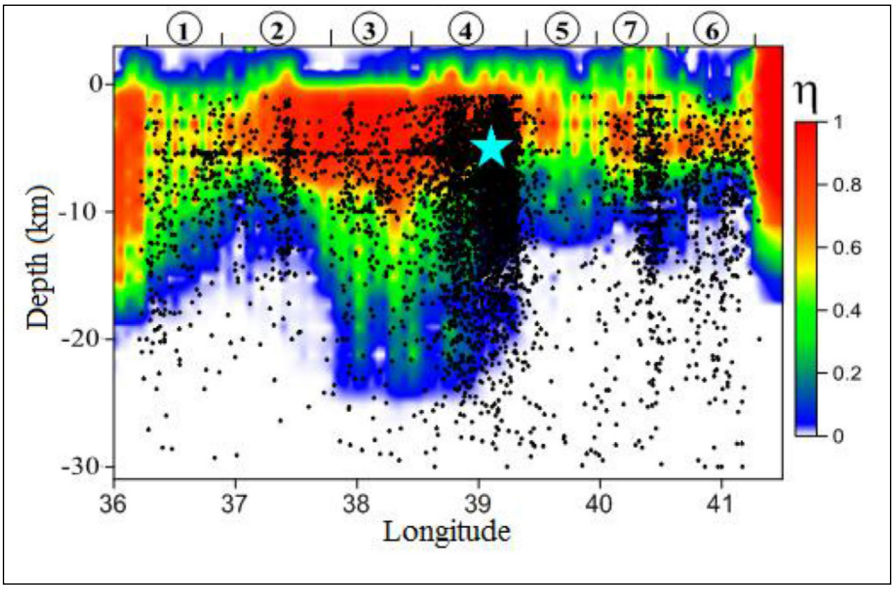

Figure 17- The change of frequency dependency degree (h) values along the EAFZ. Here, the black dots indicate the focal distribution of the earthquakes occurring along the zone, while the blue star indicates the focal point of the January 24, 2020 Elazığ-Sivrice earthquake. Numbers on the cross section are the same as in Figure 12.

revealed that the results obtained from the cross - sections given in Figure 18 were consistent with the results obtained along the EAFZ and Hazar - Sincik segment, which is the most important segment of EAFZ, and its slope was shown linearly. It is demonstrated that the change in %Vp, Vp, ΔQ_v^{-1} and h clearly continued along the fault.

All these determinations are given in three dimensions in figures 19, 20 and 21. The changes in %Vp, ΔQ_p^{-1} and h values are revealed more clearly. It is clearly seen that the decrease in the %Vp and the increase in Vp values are in the Hatay region, in segment number 2, in Hazar - Sincik and in Bingöl - Karlıova segment which is segment number 6 (Figure 19). Similarly, it is observed that the change in values

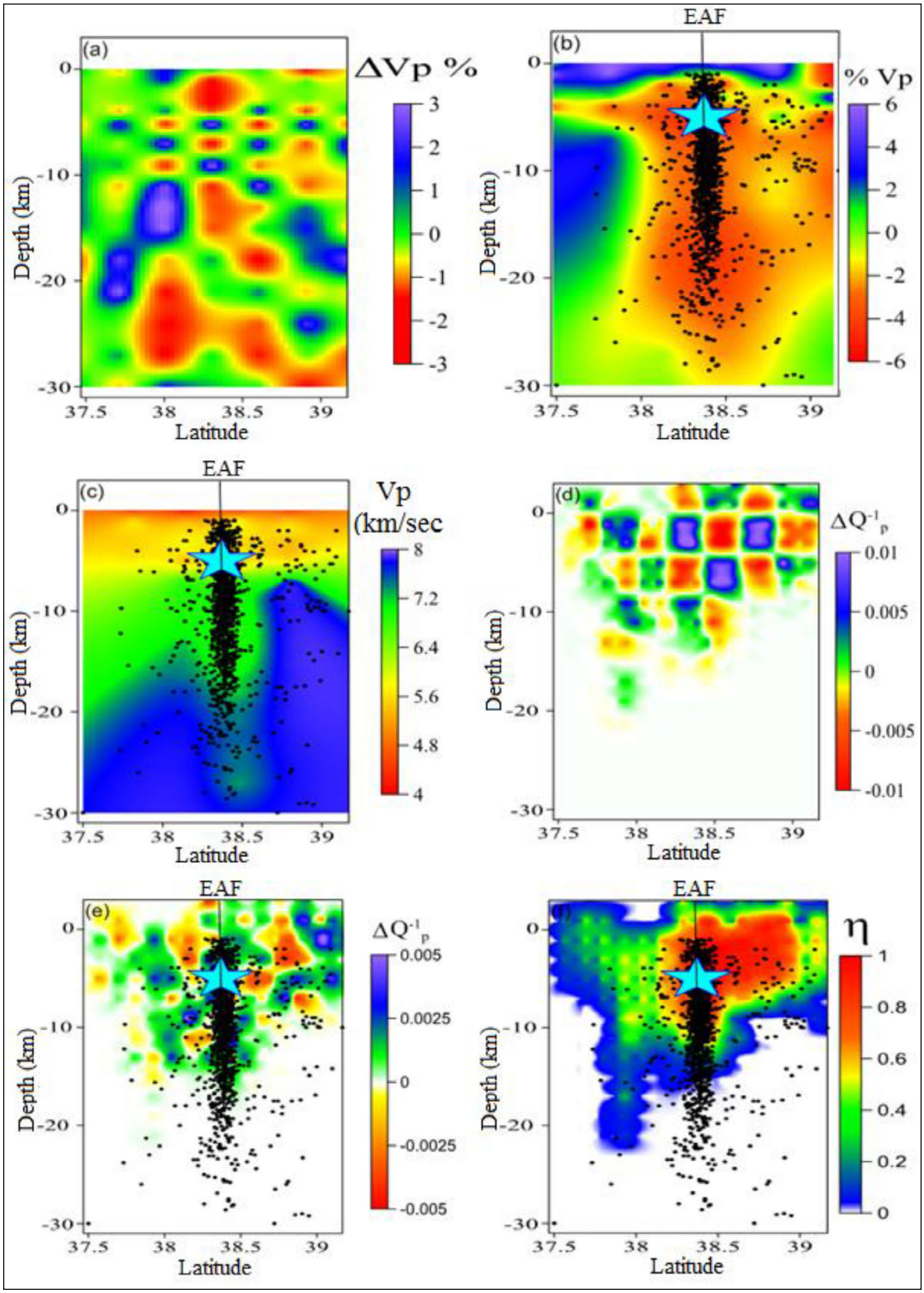

Figure 18- The change of a) DVp%, b) %Vp, c) Vp, d) ΔQ_v^{-1} checkerboard test, e) ΔQ_v^{-1} and f) η (Figure 1) along the section taken perpendicular to the Hazar-Sincik segment of the EAFZ shown as number 4 (Figure 1). Here, the black dots indicate the focal distribution of the earthquakes occurring along the section, and the blue star shows the focal point of the January 24, 2020 Elazığ-Sivrice earthquake.

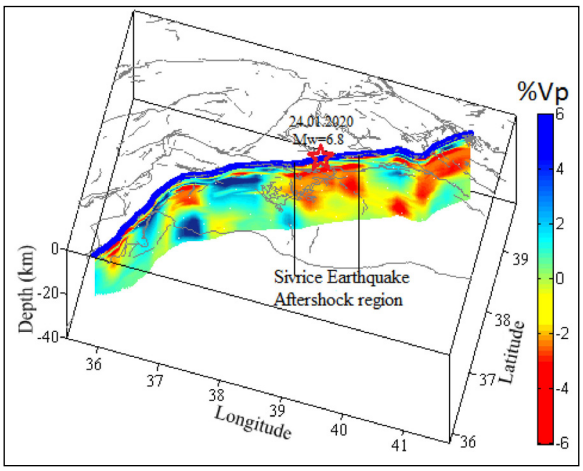

Figure 19- Three-dimensional view of %Vp change along the EAFZ. Here, the star refers to the epicenter of the January 24, 2020 Elazığ-Sivrice earthquake.

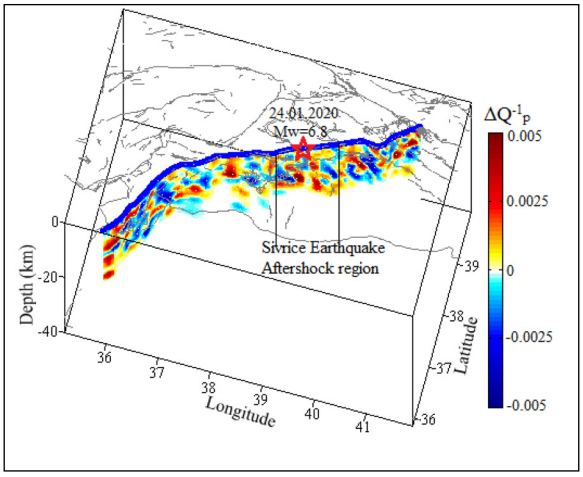

Figure 20- Three-dimensional view of the change in ΔQ_v^{-1} value along the EAFZ. The other information is the same as in Figure 19.

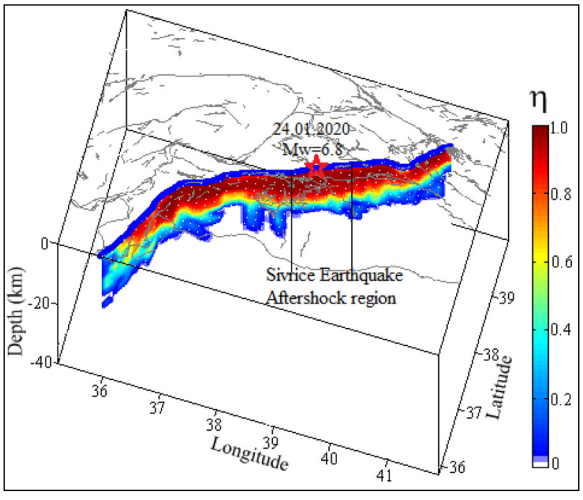

Figure 21- Three-dimensional view of the change in η value along the EAFZ. The other information is the same as in Figure 19.

of ΔQ_v^{-1} concentrates on the same segments, but differently, the value of ΔQ_p^{-1} decreases in the Yayla fault that cuts the EAFZ (MTA, 2013) (Figure 20). The fact that the maximum value in the frequency dependency level is in segment number 2 indicates that this region is in the character of an intersection, therefore it is a highly altered area. The value of h was observed in segment number 5 mostly at a depth of 15 km.

In this study, it was determined that the P wave velocity change increased up to 6% in areas near the surface and along the fault zone. While this change is higher in the fault segments as it goes deeper, it decreases in other areas. Similar results were also obtained in the studies conducted in the region. While the high P wave velocity anomalies are seen in areas close to the surface according to Salah et al. (2011), low seismic velocity anomalies are observed in deeper crustal layers. Aydın et al. (2020) stated that Vp was in the range of 6.13 - 6.49 km/sec in areas close to the surface in the region and the velocity increased towards deeper parts. It was stated by Çağlar (2019) that between 22 - 35 km depths in Hatay and its surroundings, Vp varied between 6.0 - 7.5 km/sec, and Vp greater than 7.5 km/sec was seen in areas close to the crust - mantle boundary.

It was determined that the P wave attenuation (ΔQ_p^{-1}) value varied within the range of ± 0.005 along the EAFZ. On the other hand, the degree of frequency dependency ranges from 0.1 to 1.08. Both values indicate that the region is seismotectonically active. Aydın and Kadirov (2008) determined the P wave quality factor as 28.5 where Vp was 6.25 km/sec in the region. Aydın et al. (2020) and Sertçelik (2012) examined the Coda wave attenuation pattern in the region and determined the seismic wave frequency dependency degrees as 1.25 and 0.93, respectively. These values show that the region has a high heterogeneity and is seismotectonically active.

When all these results and the 2020 Sivrice earthquake coulomb stress change (Jamalreyhani et al., 2020) are examined, the seismicity on the EAFZ should be expected to be in the Palu - Hazar segment. The change in %Vp, Vp, ΔQ_p^{-1} and h is in that direction. This situation is clearly seen in depth sections. In addition, the changes on the EAFZ will be followed with new data in order to make this study sustainable.

5. Conclusion

The three dimensional %Vp and Vp, ΔQ_v^{-1} and h values belonging to the local earthquakes recorded by 26 stations along the EAFZ were calculated by using the tomographic method to the multiple P wave arrival time inverse solution belonging to the local earthquakes recorded by 40 stations affiliated to KOREI. The checkerboard resolution test results, beam number and beam path maps show that the velocity anomalies obtained give reliable results down to a depth of approximately 30 km. Accordingly, it was observed that velocity values were generally lower than the average in some segments along the EAFZ. Regions with low %Vp anomalies are clearly visible at almost all depths. These can be interpreted as the movement of the partial melt into the crust in the lower crust and the melting mantle. It is noteworthy that although some of the earthquakes occur in high - speed regions in the region, most of them are concentrated in regions with low velocity, but in areas earthquakes with small magnitudes, active faults and high heterogeneity. Along the EAFZ, there are many sedimentary basins and widespread fault zones. The existence of low - speed zones is due to such patterns.

Velocity variations in the region show a heterogeneous pattern. It was observed that earthquakes clustered at a depth of 0 - 10 km, where the velocity changes were the greatest. However, it was observed that there was a reduction in the decrease of P wave velocity after 20 km depth. Then, the speed directly increases as the depth increases. At approximately 20 km, the wave velocity generally increases and reaches its highest level at this depth. This suggests a formation change at around 40 km.

Cross - sections were taken in two different directions in the study area, and the compatibility of these sections with respect to each other, % Vp, Vp, ΔQ_v^{-1} and h change maps were observed at the intersection points of the sections. As a result of this study, it is observed that velocity and attenuation values vary according to seismogenic limits along the EAFZ. Low Vp, high ΔQ_v^{-1} and h indicate that the environment does not lose its heterogeneity with depth and that a complex structure or upper mantle material that increases the attenuation is close to the upper part of the crust. The Vp, ΔQ_v^{-1} and h frequency dependency degree show significant changes according to the heterogeneous structure in the upper crust. These heterogeneities are shaped depending on the tectonics of the region. The high h indicates that the heterogeneity is not lost with depth, and there is a complex structure that increases the attenuation.

The data used in this study covers the period until the end of 2019. In other words, it includes the earthquake data that occurred until a time close to the 24 January 2020 Sivrice earthquake. The results obtained show that the stress accumulation was formed on the Hazar - Sincik segment where the earthquake had occurred. While the Vp value changes between 4 - 8 km/sec along the EAFZ, it was detected that it increased up to 7.5 km/sec on this segment. While the values of ΔQ_v^{-1} change within the range of ± 0.005, it is seen that it falls on the boundaries of this segment.

By adding data for the year 2020 to the existing data, it can be traced in which segment the stress accumulation occurs on the EAFZ. This situation is important for the sustainability of the study. Knowing the earthquake behavior of the EAFZ in the near future is of vital importance for the reduction of earthquake damages in the regions where many cities with a significant population and very important facilities for the economy of our country are located.

Acknowledgements

The authors thank to Wessel and Smith (1998), who prepared the GMT (Generic Mapping Tools) software used in the preparation of the figures, Prof. Orhan Dede Polat (Dokuz Eylul University, Department of Geophysical Engineering) for his contributions in the use of software, Dr. Mohamed Farouk Abdelwahed who prepared TOMOTOOLS software used in determining Vp velocity variations and to Dr. Luca De Siena who prepared MuRATv.2 used in determining the attenuation pattern.

References

Abdel - Fattah, A. K., Morsy, M., El - Hady, S., Kim, K. Y., Sami, M. 2008. Intrinsic and scattering attenuation in the crust of the Abu Dabbab area in the eastern desert of Egypt. Physics of the Earth and Planetary Interiors 168, 103-112.

AFAD, 2020. Report on 24 January 2020 Sivrice (Elazığ) Mw 6.8 Earthquake, Disaster and Emergency Management Presidency of Turkey, Ministry of Interior, Ankara, Turkey, Open File Rep. 46.

Akıncı, A. 1994. Attenuative behaviors of Western Anatolia and Southern Spain using single and Multiple

scattering models, Ph.D.Thesis, Dokuz Eylül University, Grauate School of Natural and Applied Sciences 37-39.

Akıncı, A. Eyidoğan, H. 1996. Frequency-dependent attenuation of S and coda waves in Erzincan region (Turkey) Physics of the Earth and Planetary Interiors 97, 1, 109-119 (11).

Aki, K. 1980. Scattering and attenuation of shear waves in the litosphere. Journal of Geophysical Research 85, 6496-6504.

Aki, K., Chouet, B. 1975. Origin of Coda wave: Source, attenuation and scattering effects, Journal of Geophysical Research 80, 21, 3322-3342.

Aksoy, E., İncegöz, M., Koçyiğit, A. 2007. Lake Hazar Basin: a negative flower structure on the East Anatolian Fault System (EAFS), SE Turkey. Turk. J. Earth Sci. 16, 319-338.

Allen, M., Jackson, J., Walker, R. 2004. Late Cenozoic reorganization of the Arabia-Eurasia collision and the comparison of short - term and long - term deformation rates. Tectonics 23, 1, TC2008.

Arpat, E., Şaroğlu, F. 1972. Doğu Anadolu Fayı ile ilgili bazı gözlemler. Maden Tetkik ve Arama Dergisi 78, 44-50.

Aydın, U., Kadirov, A. 2008. Erzincan ve Çevresinde P Dalgası Soğurulması. SAÜ Fen Bilimleri Dergisi 12(1), 1-8.

Aydın, U., Şahin, Ş., Kalkan, E. 2012. Yarbaşı, N., Aksoy, G., Kemaliye çevresinde Pg, Sg Soğurulması ve yeni magnitüd fomülü, Fen Bilimleri Dergisi 16, 1, 13-23.

Aydın, U., Şahin, Ş., Salah, M.K. 2020. Upper crustal Poisson's ratio and coda-wave attenuation beneath Eastern Anatolia, Earthq Eng and Eng Vib. 19, 335-347.

Barka, A. A., Kadinsky - Cade, K. 1988. Strike - slip fault geometry in Turkey and its influence on earthquake activity. Tectonophysics 7, 663-684

Bianco, F., Del Pezzo, E., Castellamo, M., Ibanez, J., Diluccio, F. 2002. Separation of intrinsic and scattering seismic attenuation in the Southern Apennine zone, Italy. Journal of Geophysical Research 150, 10-22.

Bulut, F., Bohnhoff, M., Eken, T., Janssen, C., Kılıç, T., Dresen, G. 2012. The East Anatolian Fault Zone: Seismotectonic setting and spatiotemporal characteristics of seismicity based on precise earthquake locations. J. Geophys. Res. 117, B07304, https://doi.org/10.1029/2011JB008966.

Bulut, F. 2017. Doğu Anadolu Fayı boyunca Sismik ve A-sismik Tektonik Hareketler: Hazar Gölü Doğu'sunda Sismik Boşluk mu yoksa Krip mi? AKÜ FEMÜBİD 17 015803 (257-263).

Çağlar, Ö. 2019. Determination of 3-D crustal seismic velocity structure beneath Hatay and surroundings, Journal of the Faculty of Engineering and Architecture of Gazi University 34(4), 2215-2227.

Çırmık, A.Y. 2018. Examining the crustal structures of Eastern Anatolia, using thermal gradient, heat flow, radiogenic heat production and seismic velocities (Vp and Vs) derived from Curie Point depth, Examining the crustal structures of eastern Anatolia 59, 2, 117-134.

De Siena, L., Del Pezzo, E., Bianco, F., Tramelli, A. 2009. Multiple resolution seismic attenuation imaging at Mt. Vesuvius, Physics of the Earth and Planetary Interiors 173, 17-32.

De Siena, L., Calvet, M., Watson, K. J., Jonkers A. R. T., Thomas, C. 2016. Seismic scattering and absorption mapping of debris flows, feding paths, and tectonic units at Mount St. Helens volcano, Earth and Planetary Science Letters 442, 21-31.

De Siena, L., Amoruso, A., Del Pezzo, E., Wakeford, Z., Castellano, M., Crescentini, L. 2017. Space-weighted seismic attenuation mapping of the aseismic source of Campi Flegrei 1983-1984 unrest, Geophys. Res. Lett. 44, 1740-1748, doi:10.1002/2017GL072507.

Del Pezzo, E., Bianco, F., De Siena, L., Zollo, A. 2006. Small scale shallow attenuation structure at Mt. Vesuvius. Phys. Earth Planet. Inter. 157, 257-268.

Demirtaş, R. 2003. DAFZ'nda Deprem Üreten Diri Faylar; 1900-2003 Yılları Arasında Doğu Anadolu Fay Zonunda Olmuş Hasar Yapıcı Depremler. Deprem ve Kentleşme. 23-24-25 Eylül 2003, TMMOB Jeoloji Müh. Odası yayınları 78, Konferans serisi 3.

Demirtaş, R., Erkmen, C. 2019. Doğu Anadolu Fay Sistemi Deprem Etkinliği, Gelecek Deprem Potansiyeli, Researchgate DOI: 10.13140/RG.2.2.24235.49449.

Demirsıkan, İ. H., Şahin, Ş., Öksüm, E. 2019. Orta Anadolu'da kabuğa ait sismik P ve S dalga hızı yapısının belirlenmesi, Pamukkale Üniversitesi, Mühendislik Bilimleri Dergisi 25, 6, 775-784,

Dewey, J. F., Hempton, M. R., Kidd, W. S. F., Şaroğlu, F., Şengör, A. M. C. 1986. Shortening of continental lithosphere: the neotectonics of eastern Anatolia: a young collision zone. In: Coward, M. P., Ries, A. C. (Eds.), Collision Tectonics. Geological Society, London, Special Publications 19, 3-36.

Djamour, Y., Andrnant, P., Nankali, H. R., Tavakoli, F. 2011. NW Iran-Eastern Turkey present - day kinematics:

Results from the Iranian permanent GPS network. Earth and Planetary Science Letters 307, 27-34, doi:10.1016/j.epsl.2011.04.029.

Duman, T. Y., Emre, Ö. 2013. The East Anatolian Fault: geometry, segmentation and jog characteristics, Geological Society, London, Special Publications 372, 495-529. Doi:10.1144/SP372.14.

Eken, T., Mayeda, K., Hofstetter, A., Gök, R., Örgülü, G., Turkelli, N. 2004. An Application of the Coda Methodology for Moment - Rate Spectra Using Broadband Stations in Turkey, Geophysical Research Letters 31(11): L11609. doi: https://doi.org/10.1029/2004GL019627.

Farouk, M., Zhao, D. 2006. Tomo tools programme for Windows V 1.0. Geodynamics Research Center (GRC), Ehime University, Japan, Scientific Report 1. (unpublished).

Ford, S. R., Phillips, W.S., Walter, W. R., Pasyanos, M. E., Mayeda, K., Dreger, D. S. 2010. Attenuation Tomography of the Yellow Sea / Korean Peninsula from Coda - source normalized and direct Lg Amplitudes. Pure Appl. Geophys 167, 1163-1170.

Frenkal, A., Mcgarr, A., Bicknell, J., Mri, J., Seeber, L., Cranswick, E. 1990. Attenuation of high-frequency shear waves in the crust: measurements from New York State, South Africa and Southern California. Journal of Geophysical Research 95, 17441-17457.

Hempton, M.R. 1985. Structure and deformation history of the Bitlis sture near Lake Hazar, south eastern Turkey. Geol. Soc. Am. Bull. 96, 233-243.

Herece, E. 2003. Doğu Anadolu Fayı. Antakya ve Osmaniye'nin Depremselliği ve Kentleşmeye Etkileri. 26-27 Haziran 2003, TMMOB Jeoloji Müh. Odası yayınları 76, Konferans serisi 1.

Herece, E., Akay, E. 1992. Karlıova - Çelikhan arasında Doğu Anadolu Fayı, Türkiye 9. Petrol Kongresi, 361-372.

Horasan, G., Boztepe - Güney, A. 2004. S-wave attenuation in the Sea of Marmara, Turkey, Phys. Earth Planet. Interiors 142, 215-224.

Ibanez, J. M., Del Pezzo, E. D., Miguel, F., Herraiz, M., Alguacil, G., Morales, J. 1990. Depth - dependent seismic attenuation in the Granada zone (South Spain). Bull. Seismol. Soc. Am. 80, 1232-1244.

İmamoğlu, M. Ş., Çetin, E. 2007. Güneydoğu Anadolu Bölgesi ve yakın yöresinin depremselliği, D.Ü. Ziya Gökalp Eğitim Fakültesi Dergisi 9, 93-103.

Jamalreyhani, M., Büyükakpınar, P., Cesca, S., Dahm, T., Sudhaus, H., Rezapour, M., Isken, M. P., Asayesh, B. M., Heimann, S. 2020. Seismicity related to the eastern sector of Anatolian escape tectonic: the example of the 24 January 2020 Mw 6.77 Elazığ-Sivrice earthquake. Solid Earth, https://doi.org/10.5194/se-2020-55.

Jordan, T., Chen, Y., Gasparani, P., Madariaga, R., Main, I., Marzocchi, W., Papadopoulos, G., Sobolev, G., Yamaoka, K., Zcchau, J. 2011. Operational earthquake forecasting: State of knowledge and guidelines for utilization. Annals of Geophysics 54, 4. doi: 10.4401/ag-5350

Kalafat, D., Gürbüz, C., Üçer, S.B. 1987. Batı Türkiye'de Kabuk ve Üst Manto Yapısının Araştırılması. Deprem Araştırma Bülteni 59, 43-64.

Kartal, R. F., Kadiroğlu, F. T. 2013. Doğu Anadolu Fayının sismotektoniği ve bu fay üzerindeki son beş yıllık deprem aktivitesinin istatistiksel analizi, 66. Türkiye Jeoloji Kurultayı 01-05 Nisan 2013, ODTÜ Kültür ve Kongre Merkezi, Ankara.

KOERI, 2020. Kandilli Observatory and Earthquake Research Institute, Dataset / Seismic Network. doi: 10.7914/SN/KO, Çengelköy, İstanbul, http://www.koeri.boun.edu.tr. January 30, 2020.

Melgar, D., Ganas, A., Taymaz, T., Valkaniotis, S., Crowell, B.W., Kapetanidis, V., Tsironi, V., Yolsl-Çevikbilen, S., Öcalan, T. 2020. Rupture Kinematics of January 24, 2020 Mw 6.7 Doğanyol-Sivrice, Turkey Earthquake on the East Anatolian Fault Zone Imaged by Space Geodesy, Manuscript submitted to, Earth and Planetary Science Letters, DOI: 10.31223/osf.io/xzg9c.

Mc Kenzie, D. P. 1976. The East Anatolian Fault, a major structure in Eastern Turkey. Earth and Planetory Sciences 29, 189-193.

Mohanty, W. K., Prakash, R., Suresh, G., Shukla, A. K., Walling, M. Y., Srivastava, J. P. 2009. Estimation of Coda wave attenuation for the National Capital Region, Delhi, India, using local earthquakes, Pure and Applied Geophysics 166(3), 429-449.

MTA. 2013. Türkiye Diri Fay Haritası. Maden Tetkik Arama Genel Müdürlüğü, Ankara.

Mukhopadhyay, S., Sharma, J. 2010. Attenuation characteristics of Garwhal-Kumaun Himalayas from analysis of coda of local earthquakes, Journal of Seismology 14, 693-713.

Nalbant, S., McCloskey, J., Steacy, S., Barka, A. 2002. Stree accumulation and increased seismic risk in Eastern Turkey. Earth and Planetary Science Letters 195, 291-298.

Özer, C., Gök, E,. Polat, O. 2018. Three - Dimensional Seismic Velocity Structure of the Aegean Region of Turkey from Local Earthquake Tomography, Annals of Geophysics 21(61), 2018.

Pulli, J.J. 1984. Attenuation of coda waves in New England, Bulletin of the Seismological Society of America 74, 4, 1149-1166

Reilinger, R., McClusky, S., Andrnant, P., Lawrence, S., Ergintav, S., Çakmak, R., Özener, H., Kadirov, F., Guliev, I., Stepanyan, R. 2006. GPS constraints on continental deformation in the Africa - Arabia Eurasia continental collision zone and implications for the dynamics of plate interactions. Journal of Geophysical Research: Solid Earth (1978-2012) 111, doi:10.1029/2005JB004051.

Salah, M. K., Şahin, Ş. 2019. 3D crustal velocity and *VP* / *VS* structures beneath Southeast Anatolia and their geodynamic implications, Geofizicheskiy Zhurnal 2(41), 122-140.

Salah, M. K., Şahin, Ş., Destici, C. 2007. Seismic Velocity and Poisson's Ratio Tomography of the Crust Beneath Southwest Anatolia: an Insight into the Occurrence of Large Earthquakes, Journal of Seismology 11: 415-432. DOI 10.1007/s10950-007- 9062-2.

Salah, M. K., Şahin, Ş., Aydın, U. 2011. Seismic Velocity and Poisson's Ratio Tomography of the Crust Beneath East Anatolia, Journal of Asia Earth Sciences 40, 3, 746-761.

Sato, H. 1977. Energy propagation including scattering effects single isotropic scattering approximation. Journal of Geophysical Research 25, 27-41.

Sato, H., Fehler, M.C. 1998. Seismic Wave Propagation and Scattering in the Heterogenous Earth. Springer.

Sharma, B., Kumar, D., Teotia, S. S., Rastogi, B. K., Gupta, A. K., Prajapati, S. 2011. Attenuation of Coda Waves in the Saurashtra Region, Gujarat (India) Pure Appl. Geophys. doi:10.1007/s00024-011-0295-1.

Sertçelik, F. 2012. Estimation of Coda Wave Attenuation in the East Anatolia Fault Zone, Turkey. Pure Appl. Geophys. 169, 1189-1204, https://doi.org/10.1007/s00024-011-0368-1

Şahin, Ş., Alptekin, Ö. 2003. Güneybatı Anadolu'da kabuk ve üst mantoda sismik dalgaların frekans bağımlı soğurulması. Yerbilimleri 27(2), 53-62

Şahin, Ş., Öksüm, E. 2020. Determination of Volcanic Structures in andaround Nevşehir by Seismic Attenuation Method. Journal of the Faculty of Engineering and Architecture of Gazi University 35:1, 181-191.

Şaroğlu, F., Emre, Ö., Kuşçu, İ. 1992. The East Anatolian Fault Zone of Turkey. Annal. Tecn. 6, 99-125.

Toker, M., Şahin, Ş. 2019. Crustal Poisson's ratio tomography and velocity modeling across tectono-magmatic lake regions of Eastern Anatolia (Turkey): New geophysical constraints for crustal tectonics, Journal of Geodynamics 131, 101651, 1-28.

Taymaz, T., Eyidoğan, H., Jackson, J.A. 1991. Source Parameters of large earthquakes in the East Anatolian Fault Zone (Turkey). Geophysical Journal International - Oxford 106, 537-550.

Thurber, C. H. 1987. Seismic structure and tectonics of Kilauea volcano Hawaii. In: Decker, R. W., Wright, T. L., Stau§er, P. H. (Eds.), Volcanism in Hawaii. US Geological Survey, 919ñ934.

Turkelli, N., Sandvol, E., Zor, E., Gök, R., Bekler, T., Al-Lazki, A., Karabulut, H., Kuleli, S., Eken, T., Gürbüz, C., Bayraktutan, S., Seber, D., Barazangi, M. 2003. Seismogenic Zones in Eastern Turkey, Geophysical Research Letters 30(24), 8039. doi:10.1029/2003GL018023.

Um, J., Thurber, C. H. 1987. A fast algorithm for two-point seismic ray tracing. Bull. Seism. Soc. Am. 77, 972-986.

Wessel, P., Smith, W. H. F. 1998. New improved version of Generic Mapping Tools released. EOS Trans Am Geophys U 79, 579.

Yalçın, H., Gülen, L., Çağnan, Z., Kalafat, D. 2012. Kıbrıs ve Yakın Çevresinin Depremselliği. 65. Jeoloji Kurultayı, Bildiri Özetleri Kitabı, 4-5. Ankara.

Zhao, D., Hasegawa, A., Horiuchi, S. 1992. Tomographic imaging of P- and S- wave velocity structure beneath north eastern Japan. Journal of Geophysical Research 97, 19909-19928.

Zhao, D., Hasegawa, A., Kanamori, H., 1994. Deep structure of Japan subduction zone as derived from local, regional and teleseismic events. Journal of Geophysical Research 99, 22313-22329.

Zor, E., Sandvol, E., Xie, J., Türkelli, N., Mitchell, B., Gasanov, A.H., Yetirmishli, G. 2007. Crustal Attenuation Within the Turkish Plateau and Surrounding Regions, Bulletin of the Seismological Society of America 97, 1B, 151–161.